Journal of Sound and Vibration (1997) **208**(3), 349–366

A MODIFIED PASSIVE TUNED ABSORBER FOR SECONDARY SYSTEMS UNDER RANDOM EXCITATION

S. Ma and S. E. Semercigil

Victoria University of Technology, *Mechanical Engineering Department*, *Footscray Campus*, *PO Box* 14428, *MCMC Melbourne*, *Victoria* 8001, *Australia*

(*Received* 11 *September* 1995, *and in final form* 30 *May* 1997)

Secondary systems may have to endure severe vibration amplitudes under the influence of the primary structures on which they are mounted. A series of numerical case studies are presented in this paper to investigate the effectiveness of a tuned vibration absorber with an impact damper, to attenuate the excessive vibration amplitudes of light secondary systems. In addition, experimental measurements are reported for some selective cases and comparisons are made with numerical predictions. This suggested configuration seems suited ideally as an add-on enhancer for existing conventional absorbers. Results are presented for random white noise excitation.

1. INTRODUCTION

The term ''secondary system'' is used generically for light structures which are under some influence of larger primary structures. Therefore, the response of a light secondary structure is an indirect one through the dynamic response of the primary structure to an external disturbance. Flexibly mounted machinery, transport of delicate cargo or the piping system in buildings may be envisaged as examples of secondary systems. Prediction and control of the excessive dynamic response of secondary systems have attracted attention in the literature [1–5]. A new approach of combining rather conventional two passive controllers will be investigated in this study.

Tuned vibration absorbers have been used effectively to control excessive vibrations of resonant systems [5, 6]. A tuned absorber is an auxiliary oscillator added to the primary system to be controlled. The purpose here is to interact strongly with the primary structure and to absorb the energy input from the external disturbance. Control is accomplished by tuning the parameters of the auxiliary oscillator such that an opposite force to the external disturbance is generated by intentionally resonating the absorber. Control may be very effective in restraining vibration amplitudes at the tuning frequency. However, effectiveness of a conventional tuned absorber deteriorates rapidly as the frequency of oscillations differs from this critical tuning frequency.

Many practical applications expose dynamic systems to wide band excitations, rather than single frequency excitations. Naturally, a passive conventional tuned absorber is inadequate for such cases. Some other means are required to improve the performance of the conventional tuned absorber. Active interference to maintain the resonance condition for the auxiliary absorber system promises to be effective for varying frequencies [7]. However, the approach taken in this study is to attempt to improve the performance by passive means only. Passive systems have the unquestionable advantage of simplicity and

0022–460X/97/480349 + 18 $25.00/0/sv971170

robustness, provided that they are effective. It has been demonstrated that the effectiveness of a passive tuned absorber could be enhanced significantly if another passive vibration controller, an impact damper, is used to complement the tuned absorber [8, 9].

An impact damper is a loose rigid mass placed in a container which is secured to a resonant system to be controlled. The dimensions of the container are chosen such that there is an intentional clearance around the impact damper to allow intermittent collisions. Each collision dissipates some energy and imposes an exchange of momentum. As a result of this exchange of momentum, the smaller impact damper reserves its direction of motion. On the other hand, the larger primary mass only slows down due to the momentum it lost to the damper. Control is the consequence of this slowing of the primary mass, leading to a smaller excursion amplitude. An impact damper's effectiveness largely depends upon the proper choice of the clearance. Reference [10] outlines the general approach in designing an impact damper, presents information in the form of design charts and lists relevant references.

An impact damper will be used in this study to enhance the vibration control ability of a tuned absorber. The impact damper will be placed in the tuned absorber to control the secondary system. As mentioned earlier, the concept of using these two passive controllers to complement each other's deficiencies has been introduced earlier in references [8] and [9]. Therefore, the purpose here is to extend its use in secondary systems and to provide performance charts for potential practical applications.

Implementing such an add-on enhancement in practice would be a relatively simple task. The cavity required to accommodate the impact damper may be cut into the tuned absorber. Alternatively, if machining needs to be avoided, a container could be attached to the absorber to accommodate the damper. The impact damper is simply a rigid mass to be placed in this cavity. Care may need to be taken to minimize friction, as friction would reduce the relative approach speed before collision. If the impact damper could be suspended in its cavity, as it is with the case described in section 4, frictional effects could be avoided entirely.

2. NUMERICAL SIMULATIONS

The model used in numerical simulations is shown schematically in Figure 1. In this four-degree-of-freedom (4DOF) model, the first oscillator (m_1, c_1, k_1) represents the primary system excited by the disturbance $F(t)$. The smaller secondary system (m_2, c_2, k_2) is mounted on the primary system. Attention will be mostly focused on this secondary

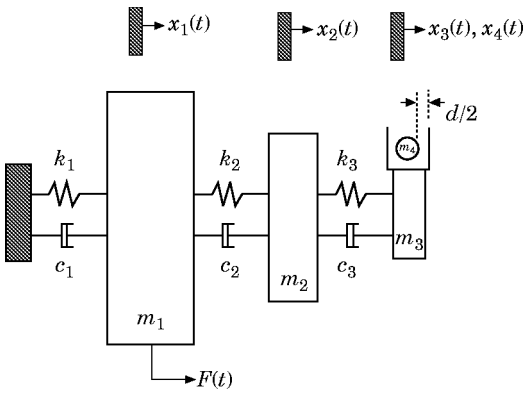

Figure 1. The three-degree-of-freedom oscillator with the impact damper.

system to restrain its response. The tuned absorber (m_3, c_3, k_3) is the auxiliary oscillator attached to m_2. Finally, the rigid mass m_4 is the impact damper. The impact damper is placed in a cavity of m_3 with a total clearance of d.

The differential equations of motion of the 3 DOF oscillator between collisions are

$$m_1 \frac{d^2x_1}{dt^2} + (c_1 + c_2)\frac{dx_1}{dt} + (k_1 + k_2)x_1 - c_2\frac{dx_2}{dt} - k_2x_2 = F(t), \tag{1}$$

$$m_2 \frac{d^2x_2}{dt^2} + (c_2 + c_3)\frac{dx_2}{dt} + (k_2 + k_3)x_2 - c_2\frac{dx_1}{dt} - k_2x_1 - c_3\frac{dx_3}{dt} - k_3x_3 = 0, \tag{2}$$

$$m_3 \frac{d^2x_3}{dt^2} + c_3\frac{dx_3}{dt} + k_3x_3 - c_3\frac{dx_2}{dt} - k_3x_2 = 0, \tag{3}$$

whereas the impact damper experiences a constant velocity motion resulting in

$$m_4 \frac{d^2x_4}{dt^2} = 0. \tag{4}$$

The numerical procedure consisted of using a standard fourth order Runge–Kutta finite difference scheme to integrate all four equations of motion simultaneously until a contact between m_3 and m_4 was established. A time step of smaller than 1/100 of the natural period of the primary system was used to ensure the stability of integration. A collision was assumed to take place when the difference between the two co-ordinates $x_3(t)$ and $x_4(t)$, was found to be smaller than one millionth of the total clearance, d, in Figure 1. Iteration on the time step was performed by bisection to locate the instant of contact.

The standard instantaneous collision assumption was used to implement the energy dissipation and momentum transfer [8]. Each collision resulted in an incremental change of velocities of the impact damper and the tuned absorber according to

$$\frac{dx_{3_+}}{dt} = \frac{(1 - \mu e)}{(1 + \mu)}\frac{dx_{3_-}}{dt} + \frac{\mu(1 + e)}{(1 + \mu)}\frac{dx_{4_-}}{dt} \tag{5}$$

and

$$\frac{dx_{4_+}}{dt} = \frac{(1 + e)}{(1 + \mu)}\frac{dx_{3_-}}{dt} + \frac{(\mu - e)}{(1 + \mu)}\frac{dx_{4_-}}{dt}, \tag{6}$$

where μ is the mass ratio (m_4/m_3) and e is the coefficient of restitution. Equations (5) and (6) may be obtained easily from the simultaneous solution of the conservation of linear momentum (before and after a collision) and from the definition of the coefficient of restitution,

$$e = -(dx_{4_+}/dt - dx_{3_+}/dt)/dx_{4_-}/dt - dx_{3_-}/dt, \tag{7}$$

where subscripts $-$ and $+$ indicate the instances immediately before and after a collision. Consistent with the instantaneous collision assumption, the displacements of m_3 and m_4 were left unchanged. A collision caused no change in the primary and the secondary systems. Numerical integration always started with zero initial conditions. After every collision, integration resumed with new initial conditions.

The random white noise excitation was approximated with [11]

$$F(t) = \sqrt{2}\sum_{k=1}^{N} [S_0(\omega_k)]^{1/2}\cos(\omega_k' t + \phi_k), \tag{8}$$

where $S_0(\omega_k)$ is the desired power spectral density of $F(t)$ with N equally spaced spectral components, $\omega_k = \Delta\omega(k - 1/2)$, $\Delta\omega = \omega_u/N$, $\omega_k' = \omega_k + \delta\omega$. $\delta\omega$ and ϕ_k are random variables uniformly distributed over the ranges of $\pm 0{\cdot}05\ \Delta\omega$ and 0 to 2π, respectively. $S_0(\omega_k)$ was taken to be unity. The cut-off frequency of the excitation, ω_u, was set to be twice as large as the natural frequency of the uncontrolled primary system with 100 spectral components (N).

Performance of the impact damper was evaluated by comparing the root mean square (rms) displacement of the secondary system between the cases with and without the impact damper. Moving rms averages were calculated after every time step until steady state. A 1000 s simulation was generally found to be long enough to obtain stationary rms averages (where the fundamental frequency of the primary system was 1 rad/s). Hence, one 1000 s long sequence of values for $F(t)$ was generated from equation (8) and this same sequence was used for each case of simulation in order to maintain consistency.

Case studies were performed for mass ratios between the secondary and the primary systems (m_1/m_2) ranging from 1 to 1000. Smaller ratios represented cases in which the primary and the secondary systems are comparable in size, whereas large ratios represented light resonant secondary structures in buildings. The natural frequency of the secondary $(k_2/m_2)^{1/2}$ and primary $(k_1/m_1)^{1/2}$ systems were taken to be identical as this case represents

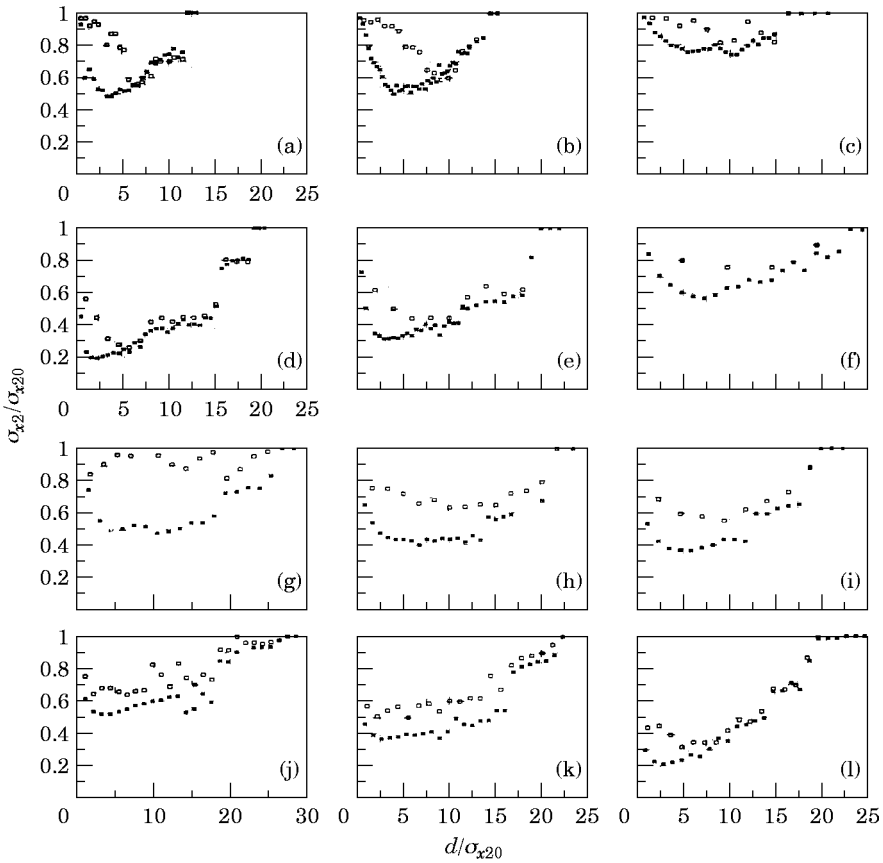

Figure 2. Variation of rms displacement ratios of the secondary system with clearance for $e = 0{\cdot}3$ (■) and $e = 0{\cdot}8$ (□) and for $m_1/m_2 = 1$ and (a) $\zeta_1 = 0{\cdot}001$, (b) $\zeta_1 = 0{\cdot}01$, (c) $\zeta_1 = 0{\cdot}05$; for $m_1/m_2 = 10$ and (d) $\zeta_1 = 0{\cdot}001$, (e) $\zeta_1 = 0{\cdot}01$, (f) $\zeta_1 = 0{\cdot}05$; for $m_1/m_2 = 100$ and (g) $\zeta_1 = 0{\cdot}001$, (h) $\zeta_1 = 0{\cdot}01$, (i) $\zeta_1 = 0{\cdot}05$; for $m_1/m_2 = 1000$ and (j) $\zeta_1 = 0{\cdot}001$, (k) $\zeta_1 = 0{\cdot}01$, (l) $\zeta_1 = 0{\cdot}05$.

the strongest interaction and hence the most critical case for the secondary system [12, 13]. The critical damping ratio of the primary system, $\zeta_1(c_1/2\sqrt{m_1k_1})$, was varied from 0 to 0·10. The secondary system was taken to be undamped ($c_2 = 0{\cdot}0$).

A mass ratio of 0·10 (m_3/m_2) was maintained between the secondary system and the absorber. The absorber was tuned to the natural frequencies of the primary and the secondary systems, $(k_3/m_3)^{1/2} = (k_2/m_2)^{1/2} = (k_1/m_1)^{1/2}$, and assumed undamped ($c_3 = 0{\cdot}0$). The mass ratio between the absorber and the impact damper, $\mu = m_4/m_3$, was kept at 0·25. Hence, although the value of μ is quite large, the addition of the impact damper raised the inertia of the secondary system only by 2·5%.

3. NUMERICAL RESULTS

In Figure 2, rms displacement ratios, σ_{x2}/σ_{x20}, of the secondary system are presented for different non-dimensional clearances, d/σ_{x20}. Here, σ_{x2} and σ_{x20} represent the rms displacement of the secondary system with and without the impact damper; and d is the total clearance of the impact damper. Hence, a σ_{x2}/σ_{x20} smaller than unity represents attenuation.

Two different coefficients of restitution, e, were used for these simulations. A value of 0·3, for instance, represents contacts between hard neoprene and metal surfaces. These results are marked with (■) in Figure 2. A coefficient of restitution of 0·8, on the other

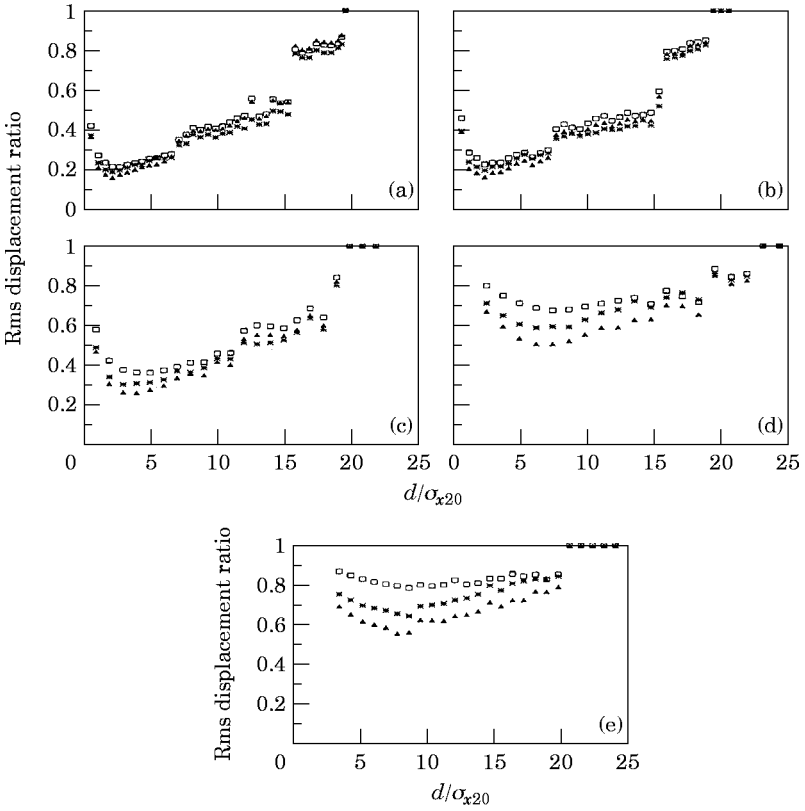

Figure 3. Variation of rms displacement ratios of the primary system σ_{x1}/σ_{x10} (□), secondary system σ_{x2}/σ_{x20} (∗) and the absorber σ_{x3}/σ_{x30} (△) for $e = 0{\cdot}3$ and for $m_1/m_2 = 10$ and (a) $\zeta_1 = 0$, (b) $\zeta_1 = 0{\cdot}001$, (c) $\zeta_1 = 0{\cdot}01$, (d) $\zeta_1 = 0{\cdot}05$ and (e) $\zeta_1 = 0{\cdot}10$.

hand, represents contacts between polished surfaces of hardened metals, such as tool steels. These results are marked with (□). For all cases presented in Figure 2, $e = 0{\cdot}3$ (■) produced more effective attenuations than those of $e = 0{\cdot}8$ (□). Hence, all further discussions will be limited to the smaller coefficient of restitution. This trend is in agreement with earlier findings reported for random excitations [14]. Different m_1/m_2 are presented in each row in a descending order, namely 1, 10, 100 and 1000. Each column corresponding to a critical damping ratio of the primary system, ζ_1, of 0·001, 0·01 and 0·05, from left to right.

Generally, all parameter combinations in Figure 2 show attenuations due to the presence of the impact damper. These attenuations are quite marginal for cases with small d/σ_{x20}, producing values of $\sigma_{x2/x20}$ close to unity. Small d/σ_{x20} cause too many collisions which mostly occur with small relative approach speeds before contact. In turn, these slow speeds drastically inhibit the momentum exchange between the impact damper and the tuned absorber. When d/σ_{x20} is large, on the other hand, too few collisions occur. As a result, attenuations were again quite insignificant. Absence of collisions due to too large a clearance is always indicated with a σ_{x2}/σ_{x20} of unity for each case. Between too small and too large clearances, results for each set of parameters indicate an optimal clearance to produce the largest attenuations. These optimal clearances produce relatively large approach speeds with an average frequency of two collisions per cycle. The term "cycle" is used loosely here due to the random nature of the disturbance.

In Figure 2, for $m_1/m_2 = 1$ and $m_1/m_2 = 10$ (in the first two rows), as the critical damping ratio of the primary system increases from 0·001 to 0·05 (from the first to the third column)

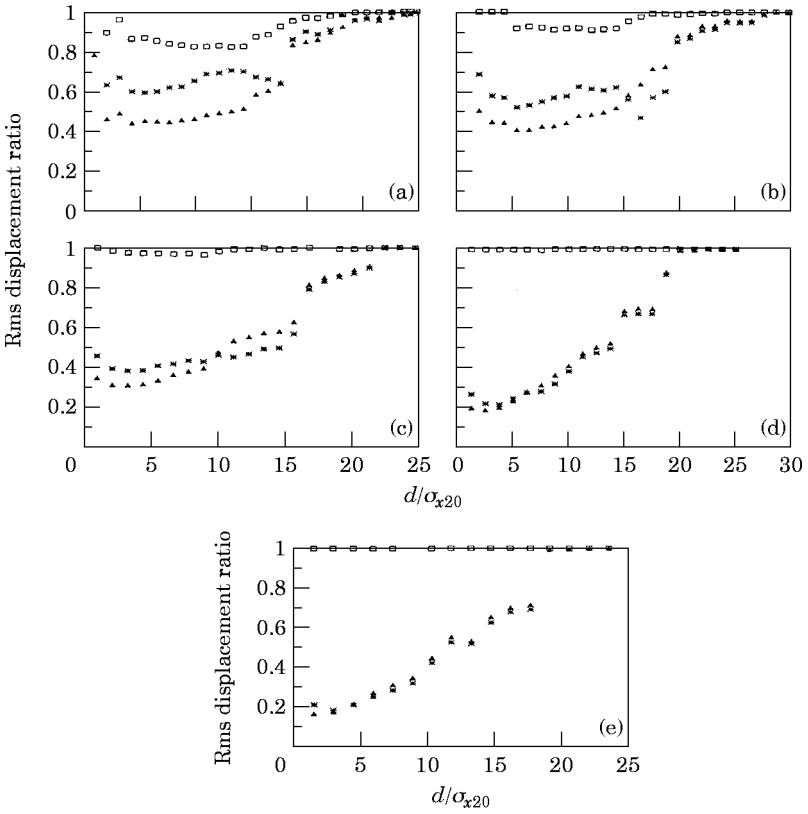

Figure 4. Same as Figure 3 but for $m_1/m_2 = 1000$.

effectiveness of the impact damper decreases. This trend is not surprising since any increase in damping will result in a smaller excursion amplitude in the absorber's oscillations. Effect of the impact damper on the secondary system is an indirect one through the response of the tuned absorber. Therefore, smaller excursions of the absorber give the impact damper less of a chance to make a difference. Best attenuations are in the order of 50% for $m_1/m_2 = 1$ and 80% for $m_1/m_2 = 10$. These attenuations deteriorate to approximately 25% and 45%, respectively, in the third column of each row.

The last two rows of Figure 2, for $m_1/m_2 = 100$ and $m_1/m_2 = 1000$, show a different trend than the first two rows. Particularly for $m_1/m_2 = 1000$, increasing values of ζ_1 produce more effective attenuations from approximately 50% in the first column to 80% in the third column. This drastic change may be attributed to the ratio of the primary and the secondary masses. When the secondary system's mass is 1000 times smaller than that of the primary system, it is virtually impossible for the primary system to be affected by changes in the response of the secondary system. Hence, excitation applied on the primary system is in fact perceived as a moving rigid base by the secondary system. Therefore, the ''apparent'' degree of freedom of the system is now reduced by one. Increasing damping in the primary system only enhances this effect.

Dependence of the attenuations of the impact damper on m_1/m_2 is demonstrated further in Figures 3 and 4. In Figure 3, the rms displacement ratios of the primary σ_{x1}/σ_{x10} ($\square$), secondary σ_{x2}/σ_{z20} ($*$) and the tuned absorber σ_{x3}/σ_{x30} ($\triangle$) systems are given for different non-dimensional clearances d/σ_{x20} but for a constant $m_1/m_2 = 10$ and for $e = 0{\cdot}3$. Each frame from 3(a–e) corresponds to a ζ_1 of 0·0, 0·001, 0·01, 0·05 and 0·10. Hence, rms ratios of the secondary system ($*$) in the middle three frames are repeated from Figure 2. Because of the relatively strong interaction between the primary and the secondary systems for this $m_1/m_2 = 10$, as the damping in the primary system increases, the relative performance of the impact damper deteriorates from approximately 80% attenuation in frames 3(a) and 3(b) to 30% in frame 3(e). What is interesting to note in Figure 3 is that, when the impact damper is effective, the attenuations are achieved in about the same order for all three of the systems simultaneously. On the other hand, when the performance deteriorates, attenuations follow the reverse order of the size of each system's mass. Larger attenuations occur for the tuned absorber, then for the secondary system and the primary system.

Results in Figure 4 are presented in a format identical to Figure 3, but this time for $m_1/m_2 = 1000$. As discussed briefly earlier, the effectiveness of control of the secondary system is particularly pronounced in Figures 4(d) and 4(e), for ζ_1 of 0·05 and 0·10, producing approximately 80% attenuation for a d/σ_{x20} range of 1·5–4. Best attenuations gradually deteriorate to approximately 65%, 50% and 40% as the value of ζ_1 changes to 0·01, 0·001 and 0·0, respectively. In Figures 4(d) and 4(e), the primary system's response remains unaffected for all clearances, whereas some marginal changes may be observed in Figures 4(a) to 4(c) due to the presence of the impact damper.

One of the drawbacks of a conventional tuned absorber is the large excursion amplitudes of the tuned absorber. Since the absorber is intentionally designed to resonate at the tuning frequency to be effective, resulting large amplitudes require sufficiently large space around the absorber and unavoidable maintenance/replacement of the absorber in time. Results presented so far invariably suggest that addition of the impact damper should negate this particular drawback.

Displacement histories of the primary, secondary and the tuned absorber are shown in Figure 5(a) for the uncontrolled system and for $m_1/m_2 = 10$ and $\zeta_1 = 0$. In Figure 5(b), the same system is shown with the impact damper and a non-dimensional clearance of $d/\sigma_{x20} = 2{\cdot}17$. The first 150 s period of the histories show the process of the gradual building of the excursion amplitudes starting from zero initial conditions. The last 150 s period, on

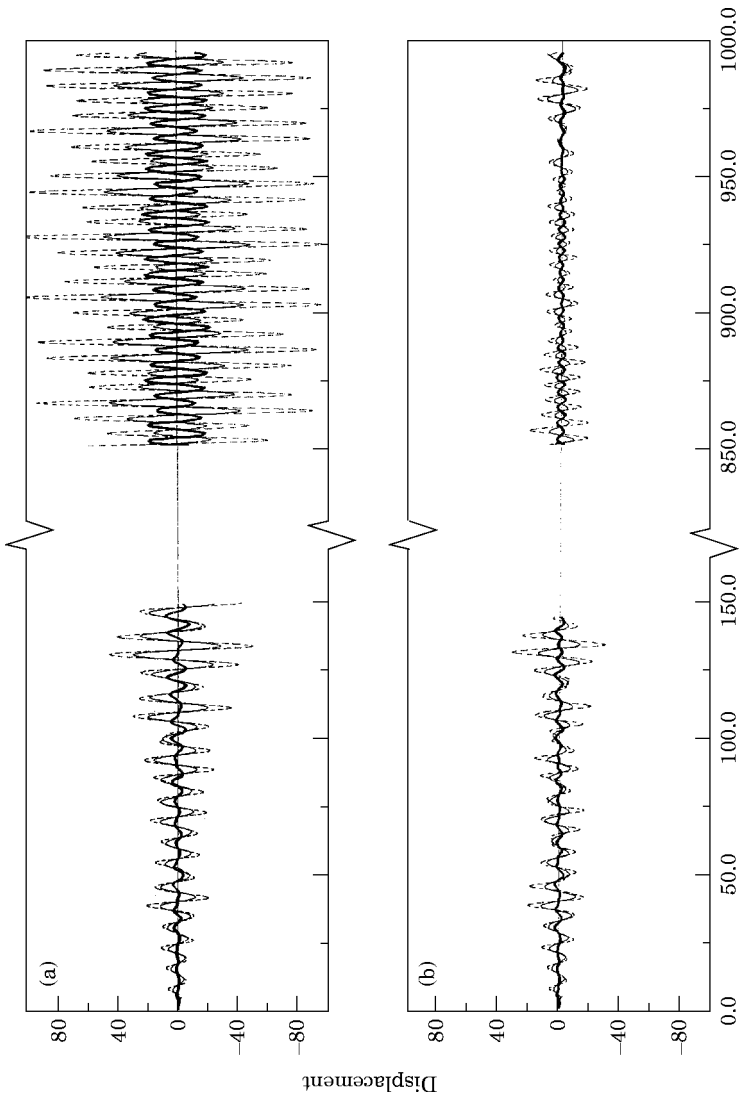

Figure 5. History of the primary (——), secondary (——) and absorber (..... .....) displacement of (a) the uncontrolled and (b) the controlled case for $d/\sigma_{x20} = 2{\cdot}17$, $m_1/m_2 = 10$ and $\zeta_1 = 0$.

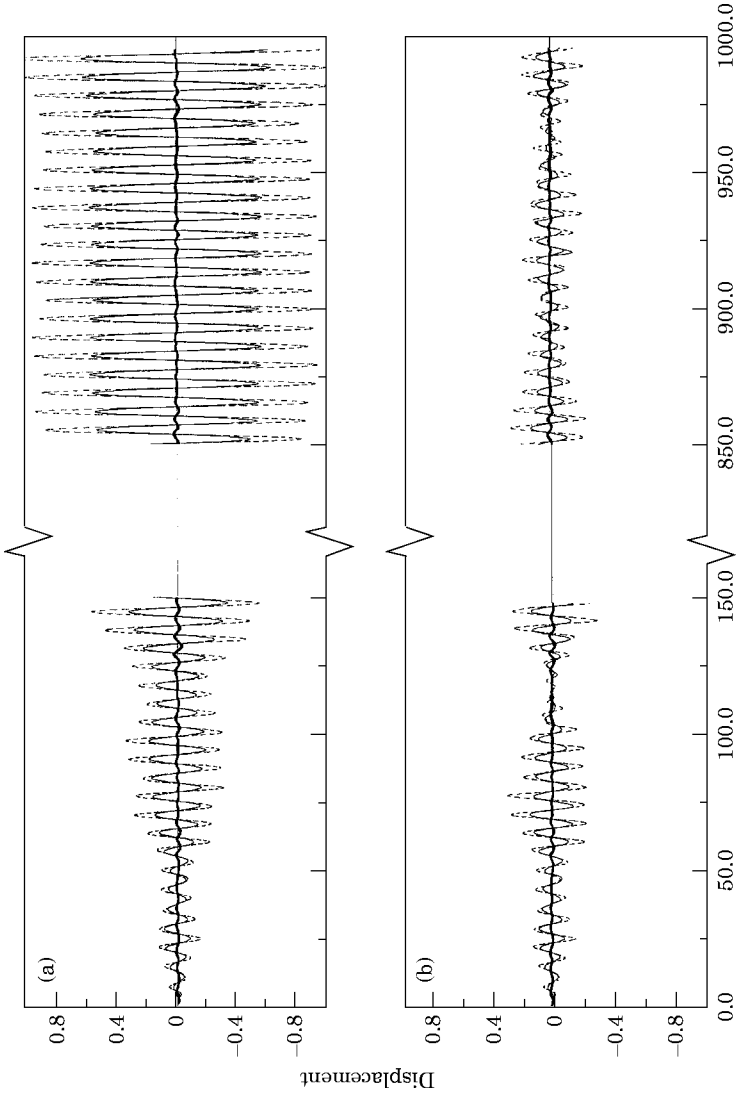

Figure 6. Same as Figure 5 but for $d/\sigma_{x20} = 2{\cdot}95$, $m_1/m_2 = 1000$ and $\zeta_1 = 0{\cdot}10$.

the other hand, exhibits an almost perfectly periodic character in response to the random white noise excitation. This periodic character is not surprising considering that an oscillator is expected to respond in a narrow band of frequencies regardless of the frequency content of the excitation. However, this natural self-organization process of deliberately picking a narrow band of preferred frequencies is a gradual one. If a randomly excited response may be envisaged as a sequence of short transient disturbances, gradual building of significantly large oscillation amplitudes require the presence of the preferred frequency components as initial conditions for each of these short transient disturbances. When this gradual building of the oscillation amplitudes is interrupted by discontinuities of the impact damper's collisions, the resulting response is somewhat disorganized and certainly smaller than the uncontrolled case [15]. Response in both Figures 5(a) and 5(b) are identical until the first contact is established at about 50 s. Differences start emerging towards the end of the initial 150 s period, though both cases are still quite similar. This similarity is due to the first few collisions having inevitably small approach speeds and being quite ineffective. However, controlled displacement amplitudes for the last 150 s are significantly smaller than those of the uncontrolled displacements. Similar comparisons may be made between the controlled and uncontrolled displacement histories in Figures 6(a) and 6(b), this time for $m_1/m_2 = 1000$, $\zeta_1 = 0{\cdot}10$ and for $d/\sigma_{x20} = 2{\cdot}95$. In Figure 6(b), controlled oscillation amplitudes of the primary system remain virtually unchanged due to its large inertia.

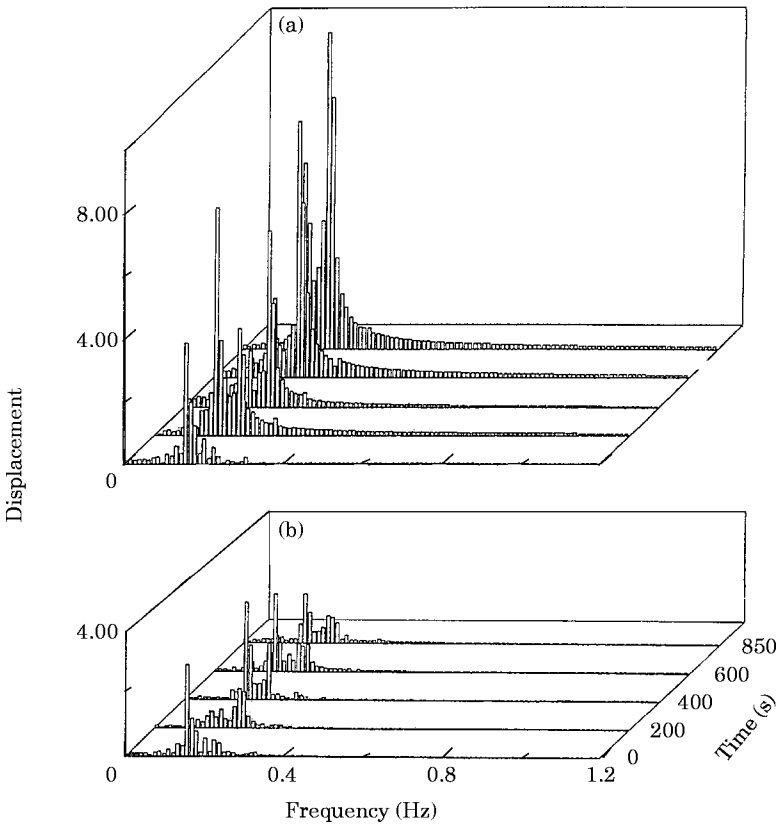

Figure 7. History of (a) uncontrolled and (b) controlled FFT of the displacement of the secondary system with $d/\sigma_{x20} = 2{\cdot}17$, $m_1/m_2 = 10$ and $\zeta_1 = 0$.

Figure 7 shows the Fast Fourier Transformation (FFT) of the displacement of the same secondary system in Figure 5. In this figure, the vertical axis represents the spectral amplitude, the horizontal axis represents frequency (in Hz) and the depth represents the starting time of a FFT snapshot (approximately 150 s long each). The top half of Figure 7 is the uncontrolled response. The gradual building process discussed earlier is displayed in this uncontrolled response, clearly emphasizing the exaggerated narrow band response after 600 s. For the first FFT, the controlled response, shown in the bottom half, has a very similar spectral distribution to that of the uncontrolled response. Starting from the second FFT, the controlled response's spectral amplitudes are significantly smaller with a wider frequency distribution. Figure 8 shows the same FFT histories in an identical format to that of Figure 7, but this time for the same parameters as in Figure 6.

Figure 9 shows the effect of the clearance of the impact damper on the displacement of the secondary system for $m_1/m_2 = 10$ and $\zeta_1 = 0$. For comparison purposes, only the last FFT snapshot (between 850 and 1000 s) of the displacement of the secondary system is shown in Figure 9(a). Some selective non-dimensional clearances, d/σ_{x20}, are marked along the depth axis. In Figure 9(a), the second FFT corresponds to the best clearance case shown earlier in Figures 5(b) and 7(b). The clearance corresponding to the fifth FFT is deliberately chosen to be too large to avoid collisions, and therefore to produce the uncontrolled response of the same case in Figures 5(a) and 7(a). As may be noted easily in this figure, too small a clearance ($d/\sigma_{x20} = 0{\cdot}54$) produces a spectral distribution with a smaller peak frequency but with a comparable spectral amplitude to that of the uncontrolled case due to having too frequent collisions. Larger clearances, on the other hand, are again ineffective due to too infrequent collisions. Example cases shown here

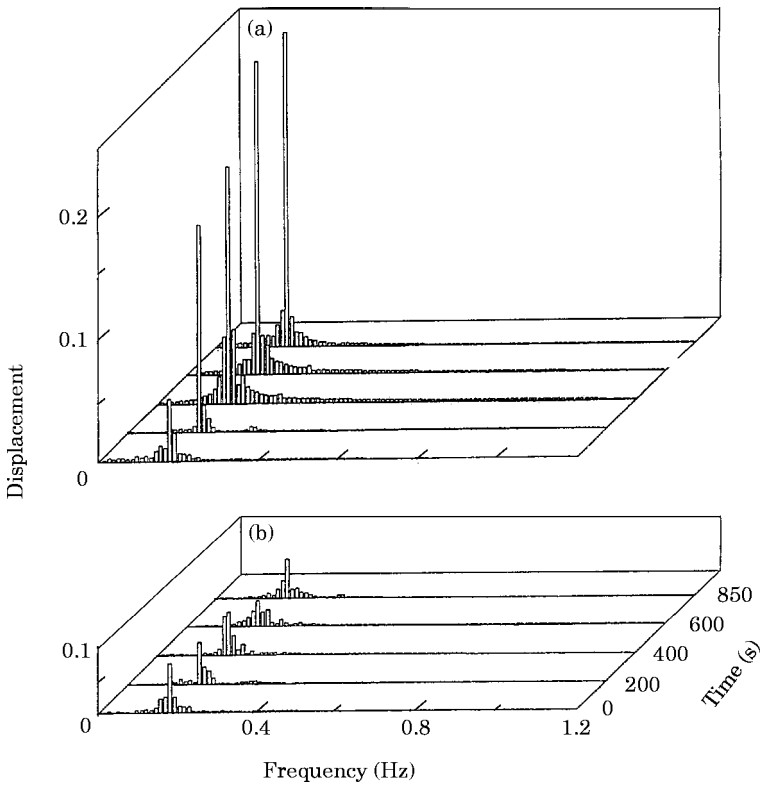

Figure 8. Same as Figure 7 but $d/\sigma_{x20} = m_1/m_2 = 1000$ and $\zeta_1 = 0{\cdot}10$.

correspond to σ_{x2}/σ_{x20} of approximately 0·37, 0·18, 0·32, 0·36 and 1·00. The same information for clearance dependence is presented this time using the probability distribution in Figure 9(b). The optimal clearance case, which is cross hatched for easy comparison, suggests a three fold attenuation of the peak displacement as comapared to the uncontrolled case. Other non-optimal clearances show similar attenuations in peak displacement to those of the corresponding rms averages.

In Figure 10, information similar to Figure 9 is presented in an identical format but for $m_1/m_2 = 1000$ and $\zeta_1 = 0{\cdot}10$. In Figure 10(a), the same comments as those made for Figure 9(a) are valid in general. The exception is that the spectral distribution of the components are significantly narrower this time due to an apparent loss of degree of freedom discussed earlier. This narrow band response leads to an almost perfectly periodic response which is reflected in the shape of the probability distribution of the uncontrolled

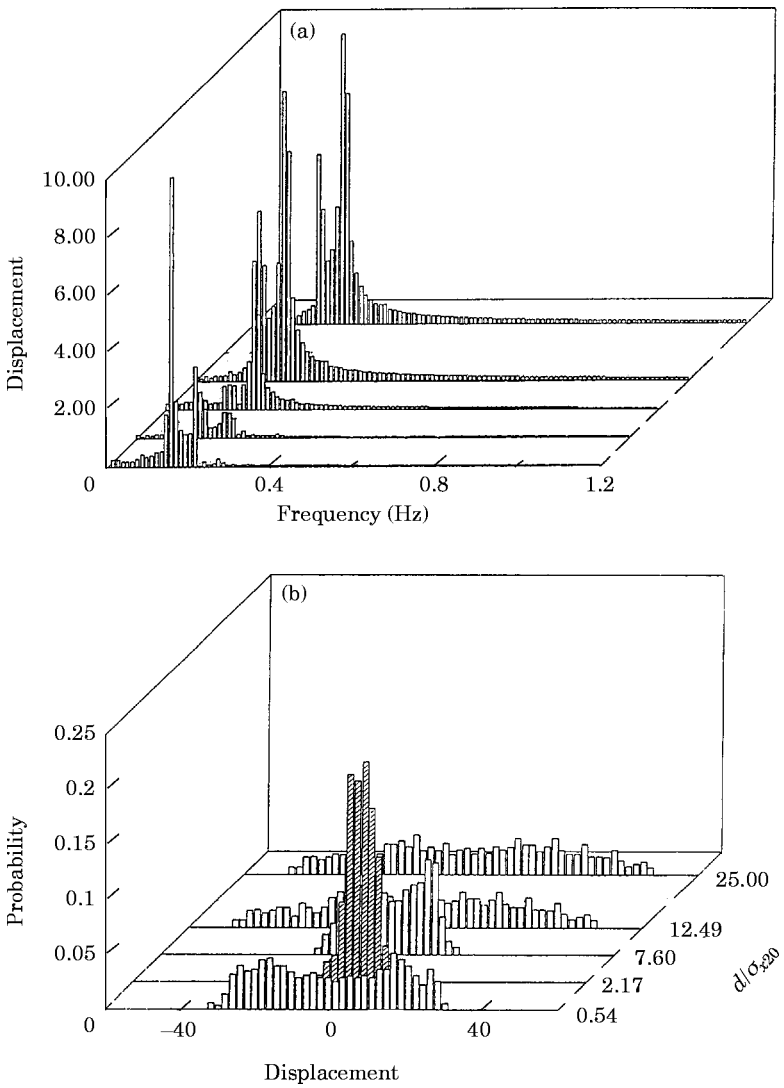

Figure 9. Variation of (a) FFT and (b) probability distribution of the displacement of the secondary system with clearance; $m_1/m_2 = 10$ and $\zeta_1 = 0$.

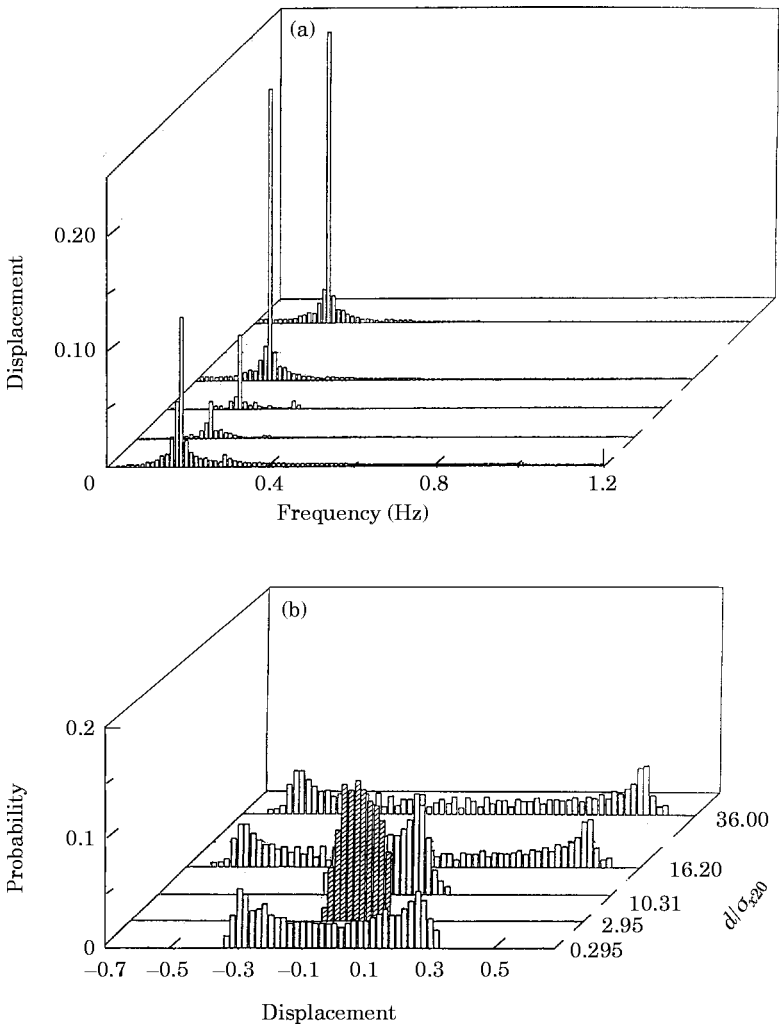

Figure 10. Same as Figure 9 but $m_1/m_2 = 1000$ and $\zeta_1 = 0{\cdot}10$.

case in Figure 10(b). This resemblance of the probability distribution to a harmonic variation may also be noticed for the first ($d/\sigma_{x20} = 0{\cdot}295$) and the fourth ($d/\sigma_{x20} = 16{\cdot}20$) clearances at varying degrees.

Another look at the attenuation mechanism of the impact damper is presented in Figure 11. In Figure 11(a), histories of the energy input to the primary system from the excitation are given for $m_1/m_2 = 10$ and $\zeta_1 = 0$ and $d/\sigma_{x20} = 2{\cdot}17$. The energy input from the random excitation seems to produce rather large fluctuations due to large velocity fluctuations of the uncontrolled system. For the optimal impact damper, on the other hand, the input energy history is much smoother as compared to the uncontrolled case. This, of course, is due to the attenuations induced in the response of the primary system by the impact damper. Surprisingly, the controlled cumulative energy input is larger than that of the uncontrolled case. Dissipated energy due to impacts, however, is just as large as the input energy, leaving only a minimal net energy.

In Figure 11(b), energy histories are presented in the same format as in Figure 11(a) but for $m_1/m_2 = 1000$, $\zeta_1 = 0{\cdot}10$ and $d/\sigma_{x20} = 2{\cdot}95$. In this figure, uncontrolled, controlled and

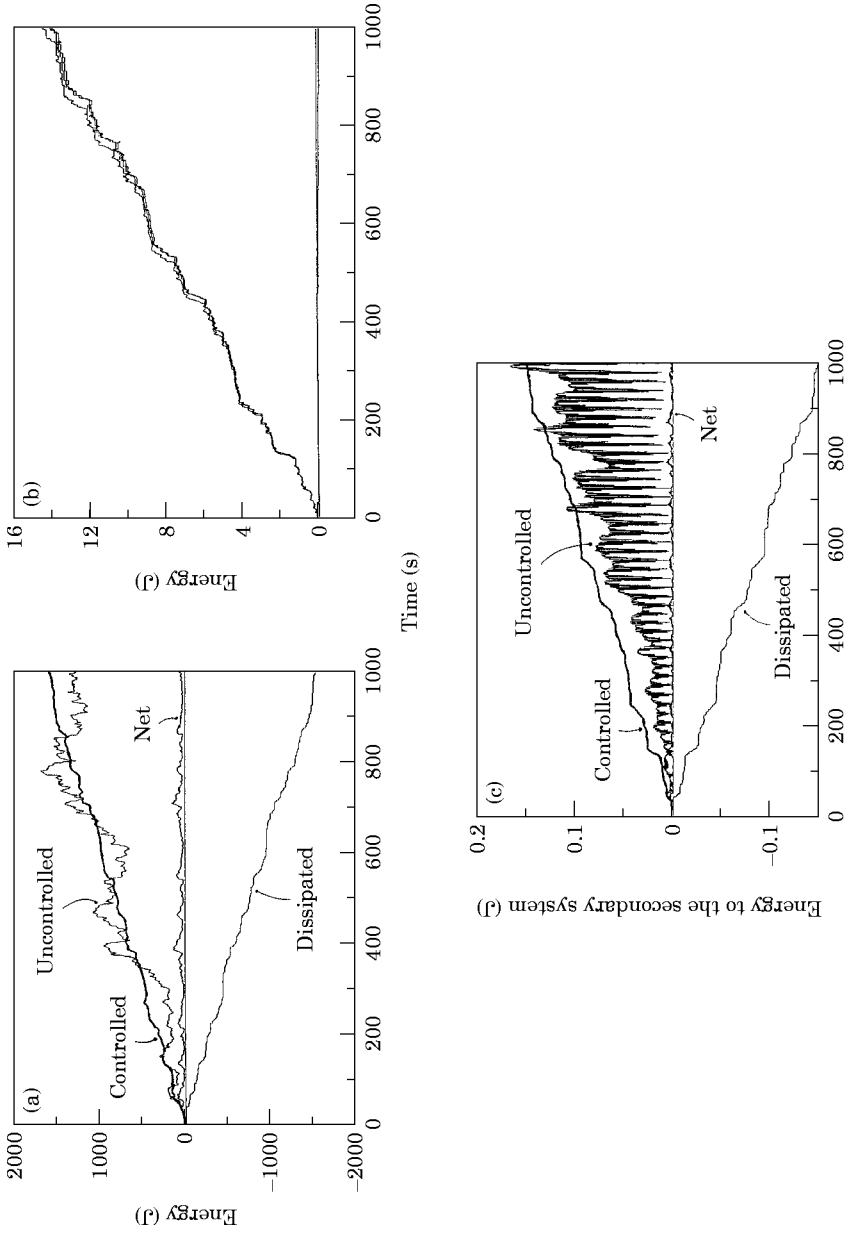

Figure 11. History of the input energy to the primary system, dissipated energy and net energy for (a) $m_1/m_2 = 10$ and $\zeta_1 = 0$, (b) $m_1/m_2 = 1000$ and $\zeta_1 = 0{\cdot}10$ and (c) same as (b) but to the secondary system.

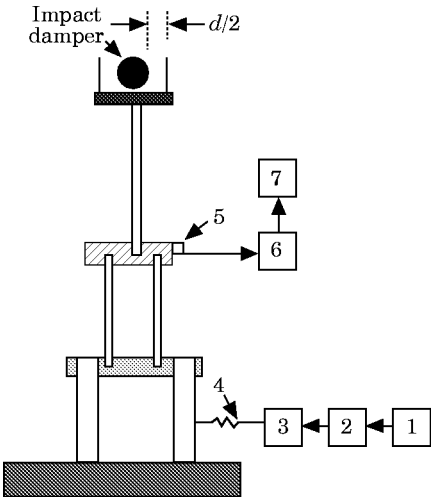

Figure 12. Experimental setup and instrumentation. 1. Brüel and Kjaer signal generator, Type 1024; 2. MB electronics amplifier, Model 2250; 3. LDS exciter, Model PM 50; 4. soft spring; 5. Brüel and Kjaer accelerometer, Type 4371; 6. Brüel and Kjaer preamplifier, Type 2625; 7. Hewlett Packard Frequency Analyzer, Type 3566A.

net-controlled energy histories seem very similar since the response of the primary system is virtually unaffected by any change in the secondary system. Histories in Figure 11(c) are for the same cases as in Figure 11(b), but this time the energy input to the secondary system rather than the primary system is plotted. Hence, this case is treated as if the primary system does not exist and the secondary system is given a base excitation. Trends in Figure 11(c) are very similar to those in Figure 11(a). Minimal net energy is left for the secondary system, after the energy dissipations due to collisions are subtracted from the energy input from the primary system.

4. EXPERIMENTS

A schematic drawing of the experimental model is shown in Figure 12. The primary structure in this model is a rigid plate cantilevered from a fixed base using thin strips of steel which act as the resilient elements as well as contributing to the equivalent mass. The secondary structure is another simple oscillator mounted on the primary structure using similar steel strips. The tuned absorber, a third oscillator, is mounted on the secondary structure. Finally, the impact damper is suspended into the cavity of the absorber by using it as the mass of a simple pendulum. Hence, the damper's motion is free of all external forces between contacts. The radial clearance, $d/2$, between the damper and the absorber is indicated in Figure 12. The parameters of the model are given in Table 1 for reference.

The experimental procedure consisted of exciting the primary system randomly by using an electromagnetic exciter, item 3 in Figure 12, which is driven by a power amplifier, item 2, and a noise generator, item 1. A soft spring was used between the exciter and the primary system to facilitate application of the random excitation. Response of the system was measured by using accelerometers attached on the primary, secondary and the tuned absorber systems (shown only on the secondary system, item 5, for clarity). The output of each accelerometer was first amplified, then processed by using a FFT analyzer which was also capable of computing the integrals of the acceleration spectra. The number of sample averages was kept high enough so that the expected error in any spectral

TABLE 1

Parameters of the experimental model: k_{eq}, ζ_{eq} and m_{eq} represent the equivalent stiffness, critical viscous damping ratio and mass when each system is considered individually as a SDOF oscillator

	Resonant Freq. (Hz)†	k_{eq}‡ (10^3 N/m)	m_{eq}‡ (kg)	ζ_{eq}†
Primary system	$25{\cdot}17 \pm 0{\cdot}35$	113·63	4·544	$0{\cdot}0053 \pm 0{\cdot}0002$
Second. system	$24{\cdot}67 \pm 0{\cdot}25$	11·22	0·467	$0{\cdot}0026 \pm 0{\cdot}0007$
Tuned absor.	$23{\cdot}08 \mp 0{\cdot}30$	1·22	0·058	$0{\cdot}0034 \pm 0{\cdot}0002$
Impact damper	—	—	0·011† $\pm 0{\cdot}005$	—

† Measured. ‡ Calculated.

component was well within 1 dB with a 90% confidence [16]. Rms amplitudes were computed by integrating the averaged spectra.

Measurements were performed over a frequency range from 0 to 50 Hz, whereas the fundamental frequency of the primary system was designed to be approximately 25 Hz. Over the frequency range, the displacement of the exciter's table showed a relatively flat spectral distribution. Hence, the excitation was assumed to be a good representation of white noise. The procedure described above was repeated with and without the presence of the impact damper. The clearance of the impact damper, d, was kept constant at $0{\cdot}190 \pm 0{\cdot}010$ mm throughout the experiments. The clearance was measured with a precision feeler gage. The coefficient of restitution between the damper and the neoprene lined (approximately 1 mm thick) walls of the tuned absorber was measured to be $0{\cdot}34 \pm 0{\cdot}05$ [9].

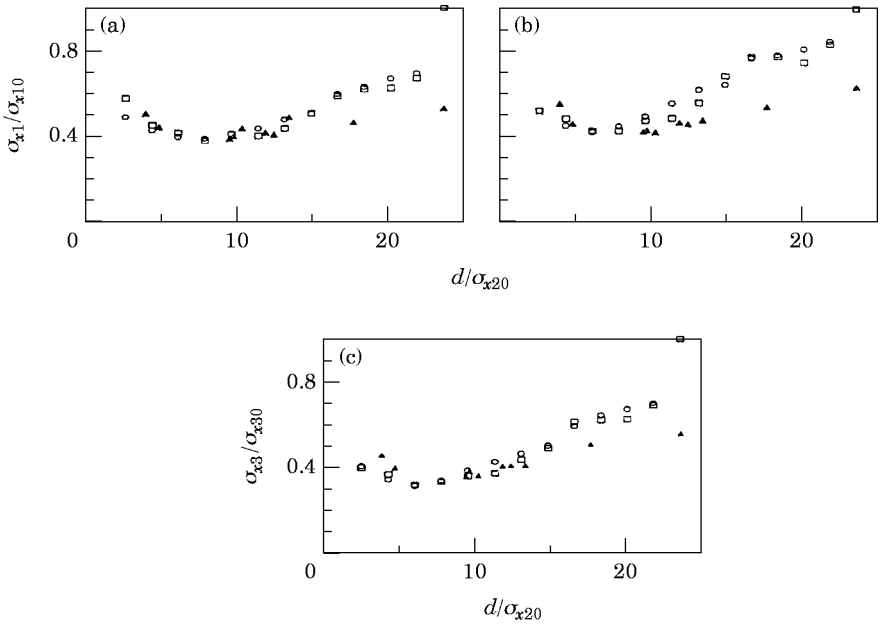

Figure 13. Comparison of the numerically predicted and measured rms displacement ratios of the (a) primary (b) secondary and (c) tuned absorber systems.

5. EXPERIMENTAL RESULTS

Both numerically predicted and experimentally observed rms displacements of the primary, secondary and tuned absorber systems are shown in Figures 13(a), 13(b) and 13(c). The vertical axis of each frame represents the corresponding non-dimensional displacement ratio, whereas the horizontal axes indicate the clearance non-dimensionalised with the rms displacement of the secondary system.

Two sets of numerical predictions are presented in this figure, considering the variation of the experimentally measured coefficient of restitution. Results for $e = 0{\cdot}3$ are shown with ($\bigcirc$), whereas ($\square$) represents results for $e = 0{\cdot}4$. Experimentally measured ratios are marked with ($\triangle$). Changing the coefficient of restitution between 0·3 and 0·4, produces quite insignificant differences. Generally, overall agreement between the numerical predictions and measurements is quite close for all three co-ordinates, particularly when the attenuations of the impact damper are most effective. This close agreement slowly deteriorates as the value of the non-dimensional clearance d/σ_{x20} increases to values greater than 13. Here, it must be kept in mind that an experimental value of the non-dimensional clearance d/σ_{x20} is varied by keeping the clearance constant and changing the level of excitation (whereas changing the clearance is a more practical approach in numerical simulations). Hence, a large d/σ_{x20} is only possible by lowering the level of excitation. At these low levels, it was found to be practically impossible to avoid the effects of small amplitude building vibrations. These structural vibrations were confounded with the practical impossibility of centering the impact damper perfectly in its cavity. Hence, at low excitation levels, more frequent collisions were observed in the experiments when compared to those predicted in numerical simulations. For small d/σ_{x20}, experimental imperfections were largely overwhelmed by high excitation levels.

6. CONCLUSIONS

Performance of a tuned absorber with an impact damper is investigated, in this study, for controlling excessive random oscillations of a light secondary system. A simple numerical procedure is presented for predicting performance under random white noise disturbance. Addition of an impact damper to a tuned absorber is a relatively simple proposition. However, this simple addition seems to provide significant improvement.

When the mass of the secondary system to be controlled is ten times smaller than the mass of the primary system, $m_1/m_2 = 10$, the impact damper is most effective when there is minimal damping in the system. Attenuations in the order of 80% are possible in the response of the secondary as well as in the primary and the tuned absorber systems. This indirect benefit of controlling the primary system through the controlled response of the secondary system, may prove particularly useful for practical applications.

When the mass of the secondary system to be controlled is thousand times smaller than the mass of the primary systems, $m_1/m_2 = 1000$, the impact damper is most effective when the primary system has at least 5% critical damping. For this case, 80% attenuation is possible for both the secondary and the tuned absorber systems. No control is attainable for the primary system due to its large inertia.

Simple experiments were performed to validate the numerical predictions. Reasonable agreement was observed between the measured and predicted results with the exception of low levels of excitation. At these low levels, the experimental model performed better than the numerical model.

Although it is not presented here, one additional benefit of employing an impact damper indirectly, is to avoid the discontinuities due to collisions. When an impact damper is placed in an oscillator directly, excursions of the oscillator may be attenuated while its

accelerations are exaggerated. This exaggeration is due to the presence of collisions. When these collisions take place in the absorber, their effect is cushioned through the dynamic response of the absorber, before reaching the secondary system to be protected. Earlier work reported comparable attenuation of accelerations to that of the displacements [9].

REFERENCES

1. A. G. Hernried and J. L. Sackman 1984 *Earthquake Engineering and Structural Dynamics* **12**, 737–748. Response of secondary systems in structures subjected to transient excitation.
2. Y. Chen and T. T. Soong 1988 *Engineering Structures* **10**, 218–228. State of the art review: seismic response of secondary systems.
3. J. M. Kelly and H. C. Tsai 1985 *Earthquake Engineering and Structural Dynamics* **13**, 711–732. Seismic response of light internal equipment in base-isolated structures.
4. N. D. Ebrahimi 1988 *Journal of Sound and Vibration* **120**, 445–455. Optimum secondary dampers for free response of underdamped systems.
5. J. B. Hunt 1979 *Dynamic Vibration Absorbers*. Letchworth, Herts: The Garden City.
6. J. C. Snowdon 1968 *Vibration and Shock in Damped Mechanical Systems*. New York: John Wiley.
7. N. Olgaç and B. T. Hol-Hansen 1994 *Journal of Sound and Vibration* **176**, 93–104. A novel active vibration absorption technique: delayed resonator.
8. S. E. Semercigil, D. Lammers and Z. Ying 1992 *Journal of Sound and Vibration* **156**, 445–459. A new tuned vibration absorber for wide-band excitations.
9. Z. Ying and S. E. Semercigil 1992 *Proceedings of Canadian Society of Mechanical Engineers CSME FORUM*, **1**, 93–98. A passive absorber for secondary systems under random excitation.
10. C. N. Bapat and S. Sankar 1985 *Journal of Sound and Vibration* **99**, 85–94. Single unit impact damper in free and forced vibration.
11. C. H. Lee and K. P. Byrne 1987 *Journal of Sound and Vibration* **119**, 529–543. Impact statistics for a random rattling system.
12. L. H. Van Berkel and S. E. Semercigil 1991 *Journal of Sound and Vibration* **150**, 322–329. Tuned vibration absorber for secondary structures.
13. A. B. Schriver and A. C. Heidebrecht 1989 *Proceedings of the Canadian Congress of Applied Mechanics*, 420–421. Damping and secondary system response.
14. S. F. Masri and A. M. Ibrahim 1973 *The Journal of the Acoustical Society of America* **53**, 200–211. Response of the impact damper to stationary random excitation.
15. S. F. Masri, R. K. Miller, T. J. Deghanyar and T. K. Caughey 1989 *Transactions of the American Society of Mechanical Engineers*, *Journal of Applied Mechanics* **56**, 658–666. Active parameter control of nonlinear vibrating structures.
16. K. G. Beauchamp 1973 *Signal Processing Using Analog and Digital Techniques*. London: Allen and Unwin.